14

Data Acquisition for Interstitial Photodynamic Therapy

Emma Henderson, Benjamin Lai and Lothar Lilge
Department of Medical Biophysics (University of Toronto)
Canada

1. Introduction

Delivery of any medical therapy needs to aim at maximizing its dose and hence impact towards the target cells, tissues, or organs while minimizing normal tissue damage to reduce morbidity and mortality to the furthest extent possible. For most procedures, monitoring of physical, chemical or biological parameters known to correlate with the therapeutic dose, and hence treatment outcome, throughout the target and adjacent tissue is thus a central aim to improve predictions of an individual's clinical outcome. The medical intervention and physical, chemical, or biological parameters correlating or predicting dose will determine the desired spatial and temporal sampling frequencies required to make accurate inferences to treatment outcome. To illustrate this concept and the limitations imposed by data acquisition as it pertains to treatment monitoring of interstitial photodynamic therapy (IPDT), or the use of light activated drugs in oncology of solid tumors, is presented in this chapter.

2. Photodynamic Therapy

Photodynamic Therapy (PDT) is the use of a drug, called a photosensitizer (PS), activated by light to achieve spatially confined or tissue-specific cell death and tissue necrosis. In general, the PS in its administered form is non-toxic and is either applied topically or administered systemically by oral route or intravenous injection. A delay period is observed in order to achieve the desired biodistribution in the target versus adjacent normal tissue, and the target is exposed to light of a wavelength absorbed by the photosensitizer (Hamblin & Mroz (2008); Davidson et al. (2010); Dolmans & Dai Fukumura (2003); Plaetzer et al. (2009)). The absorption of light photons by the photosensitizer triggers a series of photochemical reactions which, in the presence of molecular ground state oxygen in the triplet state ($^3O_2$), result in the generation of reactive oxygen species (ROS), predominantly singlet oxygen ($^1O_2$), which in turn locally damage cellular components, or the vasculature, and cause the target cells and tissue to die by necrosis or apoptosis. Thus, the conversion of the photon quantum energy by the non-toxic PS into the toxic ROS requires spatial-temporal overlap of three physico-chemical parameters: namely light photons, photosensitizer and molecular oxygen. While photon/photosensitizer overlap is intrinsic to the light fluence rate [mW· cm^{-2}] and its absorption coefficient [cm^{-1}], given by the photosensitizer's local concentration and molar extinction coefficient, the requirements on PS\$^3O_2$ spatial-temporal overlap are given by the photosensitizer's triplet state lifetime and the diffusion coefficient of oxygen in soft tissues and cells.

PDT finds a role in several stages in patient management in oncology. It is used prophylactically: in the treatment of Barrett's Esophagus, a metaplasia by stomach columnar epithelium in the squamous epithelium of the esophagus that significantly increases the probability to develop adenocarcinoma; actinic keratosis, which is associated with the development of skin cancer; or various forms of early cancer, such as of the skin, esophagus, bladder, and the oral cavity. These are excellent indications for PDT, and treatment planning or dose prescription is typically based on empirical models for administered drug concentrations [$mg \cdot kg^{-1}$] and surface light exposure [$J \cdot cm^{-2}$] of a given power density, or irradiance [$mW \cdot cm^{-2}$]. Based on considerable empirical experience this is sufficient, as none of the three known physicochemical parameters governing treatment outcome - light, photosensitizer, and $^3O_2$- exhibit significant gradients across the thickness of the lesion (typically less than 3 mm). In malignant brain tumors, it is used as an adjuvant to surgery (Popovic et al. (1996)), where the resection cavity surface is the target, reducing the problem of PDT delivery to a 2D problem. Its use as a primary treatment in large tissue volume has been investigated in the prostate (Davidson et al. (2010)). Finally, PDT is used palliatively in cases of obstructive bronchial and esophageal cancers. These successes of PDT in oncology are driving research toward broadening its application to deep-seated, solid targets (such as the prostate, as mentioned above). Such targets, however, are not accessible for surface illumination and thus require an interstitial approach for light delivery. In an effort to develop PDT as a primary treatment modality also for large volumes of solid tumour, clinical trials targeting the prostate are underway, albeit often the target is the vasculature of the prostate. PDT is in principal also an attractive treatment option for head and neck tumors, where surgery or radiotherapy may be disfiguring, as surgical extraction of the tumor requires up to 2 cm of additional tissue margins to be removed, often including bone, teeth, skin and other structures.

While for surface targets it is safe to assume ubiquitous availability of oxygen as well as homogeneous photosensitizer distribution, the same can not be assumed in solid tumors. It is widely accepted that tumors of only 1-2mm^3 can survive in an avascular environment and angiogenesis is initiated if the tumor is to continue to grow (Folkman (1974)). The angiogenesis-derived neovasculature, however, is quite disorganized, exhibiting excessive branching and long tortuous vessels that are randomly fused with either arterioles or venules, resulting in an atypical microcirculation and often a hypoxic and acidic environment. This is significant for PDT, as the efficient delivery of PS and $^3O_2$ to the target is required for a therapeutic effect and these species are no longer homogeneously available across the tumor. Indeed, treatment failure is often attributed to insufficient oxygen or a heterogeneous drug distribution (Davidson et al. (2009)). In light of these heterogeneities in the distribution of PDT efficacy determining parameters within a tumor, the same concepts of empirically derived dose metrics cannot be maintained and the spatial-temporal distribution of these parameters becomes paramount to ensure that all volume elements of the tumor target have received a sufficient dose of light, photosensitizer and oxygen to produce sufficient ($^1O_2$) causing cell death. Thus, a continuous monitoring of the real time dose-rate throughout the target volume is cardinal in enabling the desired outcome, provided at least one of the treatment determining parameters is under the control of the surgeon and can be modulated locally. While various approaches for dose-rate monitoring are possible by optical fibers or electro-polarographic probes (Chen et al. (2008)), the majority of these techniques either feature probes that sample too large an area (Weersink et al. (2005)), or require a clinically ill-advised large number of invasive probes (Li et al. (2008), Johansson (2007)).

3. Dose definitions

Keeping in mind the action mechanism of PDT, one may be tempted to choose singlet oxygen ($^1O_2$) as the dose metric, since it is the agent that is causal to cellular or vascular damage for the large majority of photosensitizers, particularly as it emits phosphorescence at 1270 nm when returning into its $^3O_2$ ground state, which can be used to quantify its concentration in a temporally resolved manner. Indeed, $^1O_2$ has been shown to correlate with the biological outcome in vitro, and singlet oxygen luminescence detection (SOLD) is a useful technique for in vitro experiments (Jarvi et al. (2006), Li et al. (2010)). For in vivo work, however, SOLD is not a feasible technique: $^1O_2$ phosphorescence has a very low quantum yield and implantable detectors with sufficient sensitivity are lacking. Two principal alternative strategies exist. The first is to deduce $^1O_2$ deposition based on the physico-chemical parameters required for its generation in PDT: light, PS, and $^3O_2$. This is termed "explicit" dosimetry, since $^1O_2$ is calculated directly from the spatial-temporal co-localization of its precursors (Wilson et al. (1997)). The second approach, "implicit" dosimetry, chooses a surrogate for $^1O_2$ - such as an interim photoproduct whose production was shown to be directly related to $^1O_2$ production (Dysart & Patterson (2006), Finlay et al. (2004)). Thus the temporal-spatial dynamics of this photoproduct imply the production of $^1O_2$ and hence the cytotoxic dose. A possible candidate metric for this approach is the excited singlet state PS ($1PS^*$), quantified through its fluorescence intensity (Pogue et al. (2008)).

In the PS fluorescence studies the spatial-temporal rate of loss in one of the efficacy determining parameters is the dose metric, whereas in the oxygen consumption model developed by T. Foster and colleagues uses oxygen depletion as the metric (Foster et al. (1991)). One disadvantage of implicit dosimetry models compared to the explicit dosimetry models is the loss of the ability to identify the *origin* of temporal-spatial variations in PDT dose, which is clinically of importance as it can lead to treatment failure when there is no appropriate correction. In explicit dosimetry the general behavior of the light fluence rate field can be obtained from a small number of spatial location measurements as the general gradient of light extinction in biological tissue is low (1-10 cm^{-1}). Local $^3O_2$ and $1PS^*$rate changes are sufficient to identify the probable efficacy-limiting parameter. The desirable spatial and temporal sampling requirements are thus given by the physical light parameters of the tissue and the intrinsic biology determining the pharmacokinetics of photosensitizer and oxygen. Table 1 provides the desired temporal and spatial sampling rates and Table 2 provides the feasible sampling rates for the PDT efficacy determining parameters. The temporal sampling rates are easily attainable for stationary probes, while the spatial requirements are not attainable for the Photosensitizer and Oxygen quantification. Improvement in the spatial monitoring is feasible using scanning probes as proposed by Zhu (Zhu et al. (2005)), but this is at the cost of the temporal sampling rates.

Explicit dosimetry involves direct measurement of the treatment efficacy-determining factors: treatment light, photosensitizer and ground state oxygen. While implicit and explicit dosimetry (Wilson et al. (1997)) are equivalent dose measures at each interrogated point in the target, explicit dosimetry permits also a dose calculation at all points in the target, based on population averages or individual tissue optical properties and pharmacokinetic parameters, prior to therapy onset. Determination of spatial gradients of these dose determining parameters can guide the medical physicist and surgeon towards modifications in the treatment plan to overcome identified obstacles to successful treatment.

Parameter	Spatial	Temporal
Fluence rate Φ	~4 cm^{-1}	~0.03 Hz
Photosensitizer concentration [PS]	0.02 μm^{-1}	~0.05 Hz
Oxygen Concentration [$^3O_2$]	0.02 μm^{-1}	~0.07 Hz

Table 1. Desired sampling rates for each PDT parameter

Parameter	Spatial	Temporal
Fluence rate Φ	< 1 cm^{-1}	< 0.5 Hz
Photosensitizer concentration [PS]	single point	< 0.5 Hz
Oxygen Concentration [$^3O_2$]	< 1 cm^{-1}	~0.5-1 Hz

Table 2. Currently technically achievable sampling for stationary sensors

The gradients are determined by the physical properties of the tissues such as the photosensitizer pharmacokinetics, oxygen perfusion versus metabolic and PDT consumption, and light absorption μ_a [cm^{-1}] and scattering μ_s [cm^{-1}] coefficients. In the following sections, the techniques used to quantify the three parameters are presented and discussed.

4. Treatment light quantification

Prior to explaining the details regarding treatment light quantification, it is important to define two quantities, irradiance and fluence rate, and their differences relevant to biophotonic applications in turbid media such as biological tissues. Although both quantities have the same units, their meanings are in fact vastly different.

Irradiance, commonly denoted ***H***, describes the power density [$mW \cdot cm^{-2}$] at a point P(x,y,z) through a surface of unit area in the direction of a surface normal **r**. Shown in the Figure 1 is a surface of unit area within an environment containing diffuse light. Irradiance is calculated by integrating all optical power through the surface that travel in the same hemisphere of **r**. In terms of clinical PDT, irradiance is the quantity of interest when an external collimated treatment light is delivered to a tissue surface such as the skin, the esophagus (van Veen et al. (2002)) or the surface of the bladder (Star et al. (2008)). Fluence rate, commonly denoted as Φ, is the three-dimensional analogue of irradiance as it describes the power density [$mW \cdot cm^{-2}$] through a sphere of unit surface area, as shown in Figure 1b. Fluence rate can be derived from irradiance by integrating irradiance through a full solid angle of 4π sr. In PDT and other light-based therapies (Robinson et al. (1998); Amabile et al. (2006)), fluence rate is used to quantify treatment light when it is delivered to a tissue volume using devices such as isotropic diffusing tip fibers. Since this delivered light travels omnidirectionally, the power delivered in all directions must be accounted for (hence the integration over 4π sr). Its gradient in tissue is determined exclusively by the effective attenuation coefficient $\mu_{eff} = \sqrt{3\mu_a(\mu_a\mu_s(1-g))}$ where $g = cos(\alpha)$, is the average cosine of the scattering angle α.

4.1 Treatment light quantification on surfaces

Irradiance on tissue surfaces can be measured with a flat photodiode detector of known area placed on the surface. If a beam larger than the detector surface is used, the fluence rate is

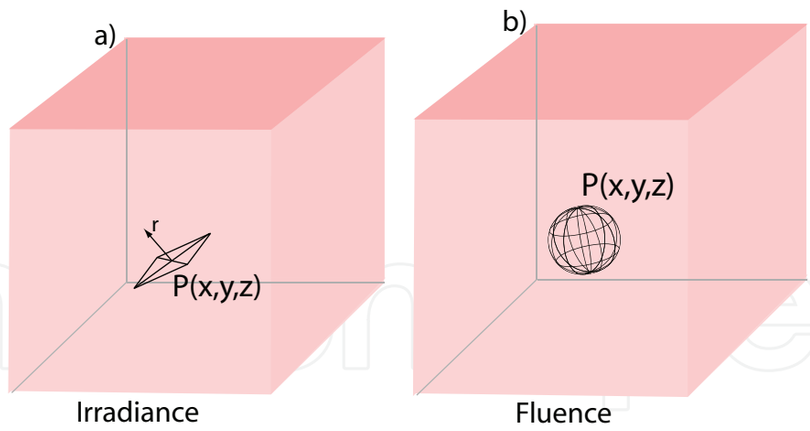

Fig. 1. The distinction between irradiance and fluence rate. The former considers optical power through a surface of unit area in a direction parallel to the surface normal (a). The latter considers the total optical power through though a sphere of unit surface area in all directions (b)

fluence rate is calculated by dividing the measured optical power by the surface area of the photodetector. Conversely, if the beam diameter is smaller, then the area of the beam is used to determine Irradiance.

4.2 Interstitial treatment light quantification

Interstitial PDT requires implanted optical fibers to deliver the treatment light to the tissue volume. These fibers may have cleaved ends (Johansson et al. (2007)), or specially designed ends with spherical or cylindrical emitting properties (Murrer et al. (1997); Vesselov et al. (2005)). Treatment light fluence rate quantification can be achieved via an additional set of embedded dedicated measurement fibers, typically cut-end (Johansson et al. (2007)), or by using the same delivery fibers reconnected to photo detectors if cut-end ((Svensson et al. (2007)) or isotropic diffusers (Yu et al. (2006); Trachtenberg et al. (2007)) are employed. The selection of the source fiber, emission and detector fiber acceptance properties and their physical separation determine the volume over which the tissue's optical properties are averaged. Thus, the use of closely spaced cut-end fibers provide the highest spatial resolution (Svensson et al. (2007; 2008)) whereas the use of a long emitter and detector (Davidson et al. (2009)) provides the lowest spatial resolution. Various existing techniques can be adapted to introduce the treatment light delivery fibers and detection fibers. For example, techniques similar to those used to implant radioactive seeds in prostate brachytherapy are employed to place the light delivery and detection fibers for prostate PDT (Weersink et al. (2005)). When using dedicated detection fibers they provide fluence rate measurements at single points, and several fibers are often necessary to obtain a useful coverage of the treatment volume (Zhu et al. (2006)).

Various approaches have been applied to reduce the number of detector fibers needed to adequately sample the target volume. One approach is to use the same delivery fibers as detection fibers, via sequential light delivery (Johansson (2007)). Another approach is to use a motorized system to translate the detector along an axis to quantify fluence rate at multiple locations, as described by Zhu et al (Zhu et al. (2005)). This technique also allows the investigators to measure the optical properties of the tissue volume in terms of the reduced scattering and absorption coefficients, since the changes in separation between light

source and detectors are known. Such information can potentially be used to provide real-time feedback so that the treatment parameters (e.g. the delivered optical power, or treatment duration) can be personalized for each patient to improve its efficacy. The collected tissue optical properties may be used to generate population averaged tissue properties, which during the treatment planning stage, are required to determine light source and detector placement.

4.3 Multi-sensor fiber probes

Multi-sensor fiber-based probes (MSP) provide another alternative to reduce the number of detection fibers thus reducing the morbidity associated with the insertion of additional catheters (Pomerleau-Dalcourt & Lilge (2006)). These MSPs still maintain the ability to simultaneously sample multiple positions without the need for a translation system. The MSPs are comprised of highly fluorescent sensor materials, commonly dyes as used in the past for dye lasers, which have been pre-selected to minimize spectral overlap. The PDT treatment light acts as the excitation source for these dyes and hence, a sensor's emission intensity is proportional to the fluence rate. The MSP fabrication process involves removing the buffer and cladding layers of the fiber then applying the sensor material onto the exposed fiber core. This allows for detection of the fluorescence via a large solid angle, maximizing the sensors' responsivity. An optically clear epoxy is mixed with a solution of the sensor material, trapping the fluorescent molecules in the matrix which has an index of refraction similar to the cladding to increase the fluorescence captured into the fiber core. When inserted into the target tissue, the fluorescence intensity of each sensor on the MSP is proportional to the localized fluence rate. Spectrally-resolved detection is required to discriminate the contribution of each sensor and determine its fluorescence intensity. Once properly calibrated, such information provides absolute fluence rate values. The downside of this MSP approach is an increase in complexity of the data acquisition and pre-processing to extract the quantity of interest, here the fluence rate Φ. The techniques used for spectral discrimination of each fluorescent sensor is described in the following section, followed by results as the MSP is evaluated in an optical phantom.

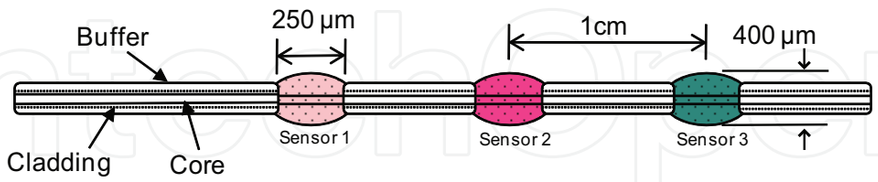

Fig. 2. Schematic of the multi-sensor probe (MSP) for spatially resolved fluence rate quantification. All sensors absorb the treatment light but emit with distinct spectra

4.4 Weighted least squares decomposition

The signal carried by the MSP fiber probe is a superposition of the individual fluorescent sensor emission. In order to obtain spatially resolved fluence rate quantification, spectrally-resolved detection is required. Since the fluorescent sensors are chosen to be spectrally distinct, a weighted least squares (WLS) algorithm is used to determine the contribution of each sensor.

Let the detected signal from the MSP be $S(\lambda)$. This quantity may be written as a sum of the contribution of each sensor with its own emission spectrum $F(\lambda)$, multiplied by a coefficient C which relates to the fluence rate of the excitation source. For simplicity, we do not consider noise due to the instrumentation, e.g. the charged coupled device (CCD) dark counts and read out noise, as well as measurement uncertainties of the data acquisition hardware. For N sensors embedded into a probe, the measured signal may be written as:

$$S(\lambda) = \sum_{i=1}^{N} C_i F_i(\lambda) \tag{1}$$

The goal is to determine C_i, which is correlated to the localized fluence rate, so that

$$S(\lambda) - \sum_{i=1}^{N} C_i F_i(\lambda) = J(C_1 \ldots C_N) \to 0 \tag{2}$$

Where $J(C_1 \ldots C_N)$ is the discrepancy function or error between the calculated and measured spectrum. Minimization of the square of this error across the entire spectral range of interest leads to a very good approximation of $S(\lambda)$:

$$\min \sum_{\lambda} \left[S(\lambda) - \sum_{i=1}^{N} C_i F_i(\lambda) \right]^2 \tag{3}$$

Minimization is typically achieved by differentiating the above equation with respect to each of the unknown values of C across the entire spectral range of interest λ. For example the jth component of the discrepancy function becomes

$$\frac{dJ}{dC_i} = 2 \sum_{\lambda} \left[S(\lambda) - \sum_{i=1}^{N} C_i F_i(\lambda) \right] F_j(\lambda) d\lambda = 0 \tag{4}$$

To simplify the expression, define the vectors **p** and Γ:

$$p_j = \sum_{\lambda} S(\lambda) \cdot F_j(\lambda) \tag{5}$$

$$\Gamma_{ij} = \sum_{\lambda} F_i(\lambda) \cdot F_j(\lambda) \tag{6}$$

Thus, the least squares expression can be simplified to become

$$\mathrm{p} - \Gamma \mathrm{c} = 0 \tag{7}$$

The amount of overlap between sensor spectra impacts significantly whether the least square approach derives an absolute or only local minimum as the least squares $\frac{dJ}{dC_i}$ becomes very flat across the planes of similar emitters . Therefore a modification to the least squares method is applied which introduces a weighting function to suppress areas where there is significant overlap, particularly when the slopes of two or more emission profiles over a specific wavelength range are similar.

The weighting function is based on the determinant of the matrix generated by taking the inner-products of every pair of fluorophore emission spectra for the specified wavelength range, say $\lambda \pm \frac{\delta}{2}$.
Recall that the inner-product of two vectors F and P is defined as

$$\cos(\mathbf{F}\hat{}\mathbf{P}) = \frac{<\mathbf{F}\cdot\mathbf{P}>}{|\mathbf{F}|\cdot|\mathbf{P}|} = \frac{\int F(x)\cdot P(x)\cdot dx}{\sqrt{\int F^2(x)\cdot dx \cdot \int P^2(x)\cdot dx}} \quad (8)$$

For a collection of fluorescent sensors, the determinant becomes

$$k(\lambda') = \det\left[\frac{\sum_{\lambda-\delta/2}^{\lambda+\delta/2} F_i(\lambda')\cdot F_j(\lambda')}{\sum_{\lambda-\delta/2}^{\lambda+\delta/2} F_i^2(\lambda')\cdot F_j^2(\lambda')}\right] \quad (9)$$

for i = 1...N and j = 1 ... N
The value of $k(\lambda')$ approaches zero at wavelength λ' when there is significant overlap between spectra, indicating that there is no solution to satisfy the system of equations. The determinant values calculated at different wavelengths make up the weighting function $w(\lambda)$, which is introduced into the least squares system of equations to suppress areas of spectral overlap and noise. The result is emphasised regions in all spectra that are favourable to increase the likelihood of obtaining a gradient of $\frac{dJ}{dC_i}$ in all dimensions and hence a unique and correct solution for:

$$p_i = \sum_{\lambda} w(\lambda)\cdot S(\lambda)\cdot F_j(\lambda) \quad (10)$$

$$\Gamma_i = \sum_{\lambda} w(\lambda)\cdot F_i(\lambda)\cdot F_j(\lambda) \quad (11)$$

4.5 Measurement accuracy

Tissue simulating optical phantoms consisting of Intralipid, a fatty emulsion normally used for intravenous feeding, as the scattering component and napthnol green as the absorbing component were prepared to assess the measurement accuracy of the MSP and fluence rate extraction system. The desired absorbing and reduced scattering coefficients (μ_a and μ_s', respectively) were obtained based on the dilutions as described by Martelli et al (Martelli & Zaccanti (1997)). The experimental setup involved submerging the MSP after calibration into the phantom at a fixed position. A spherical isotropic diffusing tip fiber connected to a 670 nm laser source was placed at different known distances from the sensors inside the phantom to evaluate the fluence rate sensitivity and accuracy of the probe. Since the optical properties of the phantom are known and uniform througout, the fluence rate at any distance away from the isotropic light source may be calculated using the diffusion approximation of the transport equation (Wilson & Patterson (1986)) and for comparison the detected fluence rate of the MSP.
For a spherical isotropic source in an optically homogenous medium delivering total power P, the approximate fluence rate as a function of radial distance r away from the source is:

$$\Phi(r) = P \times \frac{3\mu_s'}{4\pi r} \exp(-\mu_{eff} r) \tag{12}$$

It is highly desirable in the treatment volume targeted per light source to minimize light attenuation by tissue, which reduces light penetration, and thus to maximize treatment light delivery. Typically light sources in the red and far red regions of the optical spectrum are used (above 635 nm). In this region, tissue scattering dominates over absorption and the expression for μ_{eff} can be simplified to $\mu_{\text{eff}} = \sqrt{3\mu_a\mu_s'}$ (Pogue & Patterson (2006)).
An example of the calculated and measured fluence rates from the sensors are plotted together as a function of distance from the light source for a particular experiment. The measured fluence rate behaviour agrees well with the anticipated exponential decay as described by the diffusion approximation. The overall experimentally determined measurement accuracy for the MSP is better than 0.9 for fluence rates above 15 [mW · cm^{-2}] (Lai et al. (2009)). It is noteworthy to point out that this error includes errors in the initial probe calibration as well as uncertainties in the tissue simulating phantom's optical properties, which directly impacts the gradient of the measured fluence rate as a function of distance from the source. Figure 3 shows a comparison of the theoretical anticipated fluence rate attenuation and the experimental measurements.

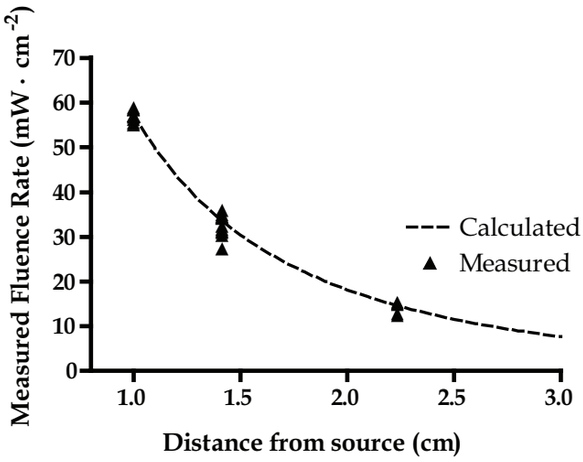

Fig. 3. Measurement of the characteristic drop in Φ(**r**) in a homogeneous optical phantom as a function of distance from the light source

5. Photosensitizer quantification

The first step in the activation of photosensitizer molecules upon absorption of a photon from the treatment light is its promotion to the singlet excited state. The photosensitizer is designed such that intersystem crossing to the triplet excited state is the preferred transition for deexcitation of the elevated singlet state. From the triplet excited state the photosensitizer is capable of interacting with ground state triplet oxygen, in an interaction which exchanges energy and electronspin thus producing singlet oxygen. However, the singlet excited photosensitizer may also return to the singlet ground state releasing a fluorescent photon with a wavelength proportional to the energy difference between the singlet ground and excited states. As a result, the fluorescence intensity may be used as an indicator of the amount of photosensitizer present in the treatment target if the excitation

intensity, here the PDT fluence rate is known at this location. This photosensitizer fluorescence may be captured to track its depletion rate and to quantify the amount of photosensitizer present for the purpose of treatment monitoring.
Quantifying fluorescence on tissue surfaces require a photo detector or a detector array (for spatially resolved fluorescence imaging) with adequate sensitivity at the fluorescence wavelength. The detection system must be equipped with the necessary filters to remove the excitation light from saturating the sensor. Additionally, prior to administration of the photosensitizer, a baseline image or spectrum should be taken to account for any autofluorescence from tissue components such as elastin and collagen in the area of interest, to prevent overestimation of the quantified fluorescence. Previous studies (Van der Veen et al. (1994); Zaak et al. (2001)) have demonstrated that fluorescent photosensitizers like ALA-induced PPIX may be imaged with a standard CCD camera to observe fluorescence kinetics of the photosensitizer during PDT treatment.
Interstitial quantification of photosensitizer fluorescence requires interstitially implanted bare-end detection fibers for point measurements. An additional level of complexity is inherent to interstitial measurements, because the tissue optical properties (absorption, scattering and anisotropy), and source detector separation must be taken into account since these factors ultimately affect the attainable fluorescence due to variations of the excitation power (Canpolat & Mourant (2000)). Such systems have been described by several investigators Axelsson et al. (2009); Canpolat & Mourant (2000)). To determine the spatial photosensitizer distribution, multiple detection fibers are required to sample multiple spatial positions. Axelsson et al. has, based on the multiple fiber approach, presented a system to perform *in vivo* photosensitizer tomography for a targeted tissue volume, the prostate. A fiber switching mechanism permits the investigator to deliver light to each of the 18 implanted fibers sequentially while its six neighbouring fibers are used collect the photosensitizer fluorescence. A total of 108 measurements are made between 54 source detector pairs, to generate fluorescence data for tomographic reconstruction. As the optical sampling volume is a function of the tissue optical properties (Pomerleau-Dalcourt & Lilge (2006)) photosensitizer probe calibration in optical phantoms approximating the population average tissue optical properties for the organ of interest is desired.
Direct quantification of weakly fluorescing photosensitizers such as TOOKAD is performed via absorption spectroscopy. Weersink et al. demonstrated this technique *in situ* in the prostate with a light delivery fiber coupled to a broad spectrum source and a fiber-based isotropic detector. Both source and detector were directed to predetermined locations in the treatment volume using a brachytherapy template to maintain a known source-detector distance (Weersink et al. (2005)). The acquired spectrum from the isotropic detector was transformed to absorbance units and fitted to previously measured absorption spectra of the drug and its aggregate to quantify the PS concentration in tissue.

6. Oxygen quantification

The polarographic Clark-type electrode (Clark et al. (1953)) is the current standard tool for measuring partial oxygen pressure (pO_2) [kPa] of tissue (Cheema et al. (2008); Swartz (2007); Pogue et al. (2001)). Its mode of operation is based on the electrochemical reduction of ground state triplet oxygen ($^3O_2$) to generate a measurable electric current proportional to the concentration of $^3O_2$ around the probe. Absolute pO_2 quantification can be made after calibrating the electrode at a known pO_2 concentration and in the absence of oxygen. One

drawback of this technology is that oxygen is consumed to generate OH^- ions during the measurement process: $O_2 + 4e^{-1} + 2H_2O \rightarrow 4OH^-$ (Lee & Tsao (1979)). As a result, the sensitivity of Clark electrodes is directly related to the pO_2 of the environment it is measuring. To gain an appreciation of the impact that this may have within the context of PDT, it is worthwhile to note that the change in pO_2 from the atmosphere to tissue is a reduction of over 20 times (Ward (2008)). Consequently, the operation of the electrode behaves as an additional "oxygen sink" that further contributes to the depletion of $^3O_2$ in an environment that already contains low levels of oxygen, contributing further to the degradation of the measurable electrical signal.

An alternative to using an electrode is to optically measure $^3O_2$. This technique relies on the ability of $^3O_2$ to effectively quench the phosphorescence of molecules in the triplet excited (T1) state (Fitzgerald et al 2001). A phosphorescent molecule in the T1 state can return to the ground state via photon production (phosphorescence) or undergo a non-radiative energy exchange with $^3O_2$. In the event that an energy exchange takes place, the phosphorescence is said to be quenched and no photon is produced. This in effect reduces the exponential decay lifetime τ [s] of the compound, which is defined as the time required for the phosphorescence intensity to fall to $1/e$ or 37% of its initial peak value. Under constant temperature and atmospheric pressure, the variation between τ and pO_2 is linear and inversely related. An optical probe with embedded phosphorescent sensors, or an optode, can be fabricated to replace the electrode for oxygen quantification. This probe requires a short wavelength light source to promote the sensor material to the T1 state and hence induce phosphorescence which can be measured to derive the pO_2. The advantage compared to the electrode is that measurement sensitivity is inversely proportional to pO_2 and $^3O_2$ is consumed at a lower rate than the electrode. Commercially available oxygen measurement systems based on oxygen quenching have been made available from Oxford Optronics in the United Kingtom under the Oxylite brand, as well as from Ocean Optics sold under the NeoFox brand name. Both systems utilize a pulsed blue LED excitation source to generate the phosphor excitation and induce emissions from sensors embedded at the tip of fiber-based probes. Such systems, however, are capable of interrogating only one point at a time. Multiple fiber probes are thus required in order to perform spatially resolved pO_2 measurements, with the same limits to clinical acceptability as mentioned in previous sections.

6.1 Quantification techniques

There are two approaches to optically determine τ; in the time domain (TD), or in the frequency domain (FD). The TD method involves measuring the time needed for the phosphorescence to reach 37% of its initial intensity after induction of phosphorescence with a very short excitation pulse. The FD technique uses an amplitude modulated excitation source at a pre-selected frequency to induce a measurable shift in the phase and amplitude of the phosphorescence signal, as compared to the excitation signal. For a chosen modulation frequency ω [rad^{-1}], the relationship between τ and the phase (ϕ) and modulation index (m) are (Lakowicz & Masters (2008)):

$$\tan(\phi) = \omega\tau \tag{13}$$

and

$$m = \sqrt{1 + \omega^2\tau^2} \tag{14}$$

There are disadvantages for each approach in determining τ. For example, the FD technique requires higher computational resources as signal processing is performed to determine the phase offset and amplitude changes compared to the excitation. The TD technique does not need significant signal processing, at the expense of requiring significantly faster sampling hardware to ensure sufficient data points are collected to determine the decay time. Given the availability of high speed central processing units (CPUs) equipped with multiple processing cores, the cost of acquiring hardware for signal processing is drastically lower compared to the cost of acquiring a high-speed data acquisition device. Therefore the FD technique is preferred. For example, to measure a decay time of as low as 100 μs, the TD sampling hardware must have a sampling rate of at least 1 MHz to generate 100 or more time-resolved sampled points. For the FD system to accommodate this requirement, the modulation frequency needed to induce a phase offset to 90° is 10 kHz. Even with an oversampling factor of 10, the required sampling speed for the FD system is 100 kHz, which is still one order of magnitude slower than the TD system.

6.2 Frequency domain decay lifetime quantification

A block diagram of the FD system is presented in the figure 4. A 50:50, 2x2 optical coupler is used to direct excitation light to the oxygen sensor, and to guide captured sensor emissions to the photo-multiplier tubes (PMT). The excitation source is a 405nm laser diode, intensity modulated by a laser driver whose output is controlled by a programmable signal generator. The function generator is programmed to sweep through a frequency range from 100 Hz to 1 kHz. During operation, the optical coupler directs the excitation light captured at Port 1 to ports 3 and 4. The PMT at port 3 is equipped with a 405 nm bandpass filter to monitor the excitation source to be used as the reference signal. At port 4, phosphorescence induced by the delivered excitation light is captured by the coupler and re-directed to port 2 for detection by a second PMT equipped with a 650 nm long-pass filter, which generates the emission signal.

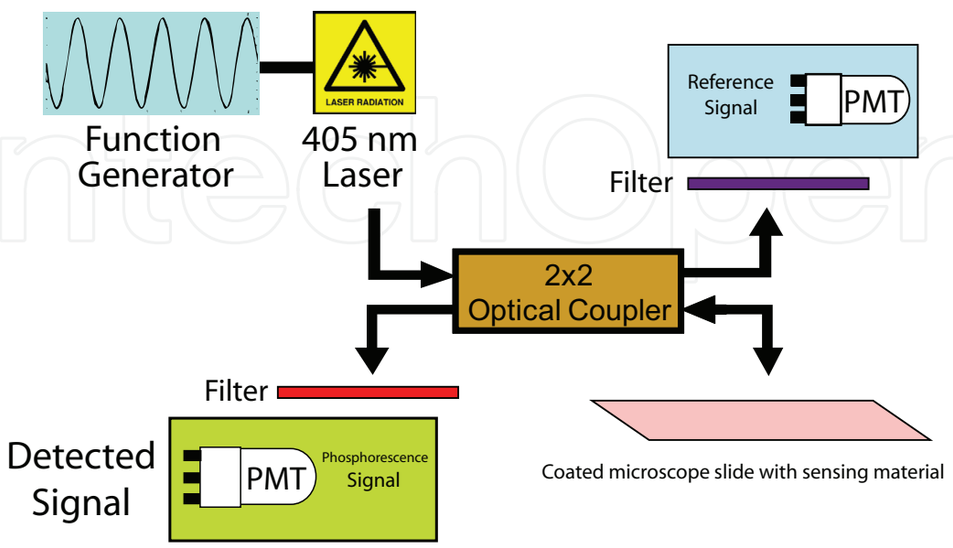

Fig. 4. Block diagram of the frequency domain system for pO^2 quantification

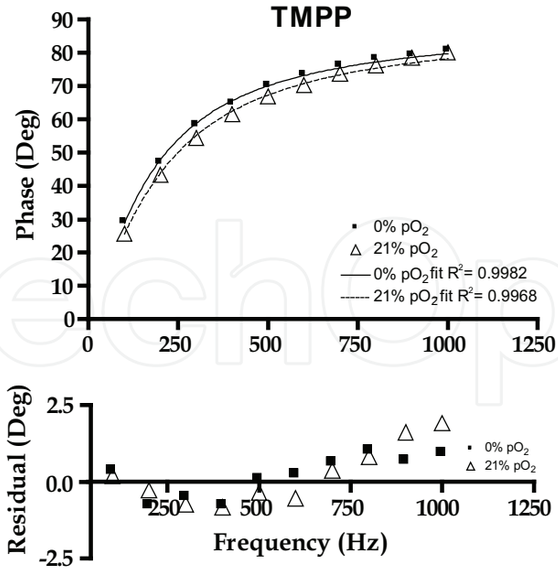

Fig. 5. Phase-frequency relationship of TMPP at 21 kPa and 0 kPa pO^2 demonstrating a change in decay lifetime

Phosphorescent palladium metalloporphyrin compound Pd-meso-Tetra(N-Methyl-4-Pyridyl) Porphine "TMPP" is used as the sensing material because of its long and measurable decay times in the μs range (Fitzgerald et al 2001). The compound is mixed into a compatible epoxy, spincoated onto a glass microscope slide, and allowed to cure. The decay lifetime of 760 μs at 21 kPa (atmospheric condition) and 903 μs at 0 kPa (anoxic) pO_2 is measured with the FD system. The value of τ should be constant for all modulation frequencies as long as the pO_2 does not change. Thus, the measured phase at different modulation frequencies follows the relationshiop described in Equation 13. Figure 5 shows a plot of the measured phase against modulation frequency at 21 kPa and 0 kPa. The solid and dotted lines represent the fitting used to determine τ based on the measured phase relationship for each oxygenation level, with a resulting R^2 greater than 0.99.

7. References

Amabile, G., Rotondi, M., Chiara, G., Silvestri, A., Filippo, B., Bellastella, A. & Chiovato, L. (2006). Low-energy interstitial laser photocoagulation for treatment of nonfunctioning thyroid nodules: therapeutic outcome in relation to pretreatment and treatment parameters, *Thyroid* 16(8): 749–755.

Axelsson, J., Swartling, J. & Andersson-Engels, S. (2009). In vivo photosensitizer tomography inside the human prostate, *Optics letters* 34(3): 232–234.

Canpolat, M. & Mourant, J. R. (2000). Monitoring photosensitizer concentration by use of a fiber-optic probe with a small source-detector separation, *Appl. Opt.* 39(34): 6508–6514.
URL: *http://ao.osa.org/abstract.cfm?URI=ao-39-34-6508*

Cheema, U., Brown, R., Alp, B. & MacRobert, A. (2008). Spatially defined oxygen gradients and vascular endothelial growth factor expression in an engineered 3D cell model, *Cellular and molecular life sciences* 65(1): 177–186.

Chen, Q., Chen, H. & Hetzel, F. (2008). Tumor oxygenation changes post-photodynamic therapy, *Photochemistry and photobiology* 63(1): 128–131.

Clark, L. et al. (1953). Continuous recording of blood oxygen tensions by polarography, *Journal of Applied Physiology* 6(3): 189.

Davidson, S., Weersink, R., Haider, M., Gertner, M., Bogaards, A., Giewercer, D., Scherz, A., Sherar, M., Elhilali, M., Chin, J. et al. (2009). Treatment planning and dose analysis for interstitial photodynamic therapy of prostate cancer, *Physics in Medicine and Biology* 54: 2293.

Dolmans, D. & Dai Fukumura, R. (2003). Photodynamic therapy for cancer, *Nature Reviews Cancer* 3(5): 380–387.

Dysart, J. & Patterson, M. (2006). Photobleaching kinetics, photoproduct formation, and dose estimation during ALA induced PpIX PDT of MLL cells under well oxygenated and hypoxic conditions, *Photochemical & Photobiological Sciences* 5(1): 73–81.

Finlay, J., Mitra, S., Patterson, M. & Foster, T. (2004). Photobleaching kinetics of Photofrin in vivo and in multicell tumour spheroids indicate two simultaneous bleaching mechanisms, *Physics in medicine and biology* 49(21): 4837–4860.

Folkman, J. (1974). Tumor angiogenesis factor, *Cancer Research* 34(8): 2109.

Foster, T., Murant, R., Bryant, R., Knox, R., Gibson, S. & Hilf, R. (1991). Oxygen consumption and diffusion effects in photodynamic therapy, *Radiation research* pp. 296–303.

Hamblin, M. & Mroz, P. (2008). *Advances in Photodynamic Therapy: Basic, Translational and Clinical*, Artech House Publishers.

Jarvi, M., Niedre, M., Patterson, M. & Wilson, B. (2006). Singlet oxygen luminescence dosimetry (SOLD) for photodynamic therapy: current status, challenges and future prospects, *Photochemistry and photobiology* 82(5): 1198–1210.

Johansson, A., Axelsson, J., Andersson-Engels, S. & Swartling, J. (2007a). Realtime light dosimetry software tools for interstitial photodynamic therapy of the human prostate, *Medical physics* 34: 4309.

Johansson, A., Axelsson, J., Swartling, J., Johansson, T., lsson, S. P., Stensson, J., Einarsdóttír, M., Svanberg, K., Bendsoe, N., Kälkner, K. M., Nilsson, S., Svanberg, S. & Andersson- Engels, S. (2007b). Interstitial photodynamic therapy for primary prostate cancer incorporating real-time treatment dosimetry, *Proceedings of SPIE*, Vol. 6427, p. 64270O.

Lai, B., Loshchenov, M., Douplik, A., Rusnov, R., Jimenez-Davila, M., Netchev, G. & Lilge, L. (2009). Three-dimensional fluence rate measurement and data acquisition system for minimally invasive light therapies, *Review of Scientific Instruments* 80(043104): 043104.

Lakowicz, J. & Masters, B. (2008). Principles of fluorescence spectroscopy, *Journal of Biomedical Optics* 13: 029901.

Lee, Y. & Tsao, G. (1979). Dissolved oxygen electrodes, *Advances in Biochemical Engineering, Volume 13* pp. 35–86.

Li, B., Lin, H., Chen, D., Wang, M. & Xie, S. (2010). Detection system for singlet oxygen luminescence in photodynamic therapy, *Chinese Optics Letters* 8(1): 86–88.

Li, J., Altschuler, M., Hahn, S. & Zhu, T. (2008). Optimization of light source parameters in the photodynamic therapy of heterogeneous prostate, *Physics in medicine and biology* 53(15): 4107–4122.

Martelli, F. & Zaccanti, G. (1997). Calibration of scattering and absorption properties of a liquid diffusive medium at NIR wavelengths. CW method, *Med. Biol* 42: 825–840.

M. Fitzgerald, DB Papovsky, MA Smiddy, JP Kerry, CK O'Sullivan, DJ Buckley and GG Guilbault, Non-destructive monitoring of oxygen profiles in packaged foods using a phase-fluorimetric oxygen sensor. Journal Food Science 66 (2001), pp. 105–110

Murrer, L., Marijnissen, J. & Star, W. (1997). Improvements in the design of linear diffusers for photodynamic therapy, *Physics in Medicine and Biology* 42: 1461–1464.

Plaetzer, K., Krammer, B., Berlanda, J., Berr, F. & Kiesslich, T. (2009). Photophysics and photochemistry of photodynamic therapy: fundamental aspects, *Lasers in Medical Science* 24(2): 259–268.

Pogue, B., Braun, R., Lanzen, J., Erickson, C. & Dewhirst, M. (2001). Analysis of the Heterogeneity of pO2 Dynamics During Photodynamic Therapy with Verteporfin, *Photochemistry and Photobiology* 74(5): 700–706.

Pogue, B. & Patterson, M. (2006). Review of tissue simulating phantoms for optical spectroscopy, imaging and dosimetry, *Journal of Biomedical optics* 11: 041102.

Pogue, B., Sheng, C., Benevides, J., Forcione, D., Puricelli, B., Nishioka, N. & Hasan, T. (2008). Protoporphyrin IX fluorescence photobleaching increases with the use of fractionated irradiation in the esophagus, *Journal of Biomedical Optics* 13: 034009.

Pomerleau-Dalcourt, N. & Lilge, L. (2006). Development and characterization of multisensory fluence rate probes, *Physics in Medicine and Biology* 51: 1929.

Popovic, E., Kaye, A. & Hill, J. (1996). Photodynamic therapy of brain tumors, *Journal of Clinical Laser Medicine & Surgery* 14(5): 251–261.

Robinson, M., David, S., Parel Ing, E. et al. (1998). Interstitial laser hyperthermia model development for minimally invasive therapy of breast carcinoma, *Journal of the American College of Surgeons* 186(3): 284–292.

Sean R H Davidson *et al* Treatment planning and dose analysis for interstitial photodynamic therapy of prostate cancer 2009 *Phys. Med. Biol.* 54 2293

Star, W., Marijnissen, H., Jansen, H., Keijzer, M. & Gemert, M. (2008). Light dosimetry for photodynamic therapy by whole bladder wall irradiation, *Photochemistry and Photobiology* 46(5): 619–624.

Svensson, T., Alerstam, E., Einarsdóttír, M., Svanberg, K. & Andersson-Engels, S. (2008). Towards accurate in vivo spectroscopy of the human prostate, *Journal of Biophotonics* 1(3): 200–203.

Svensson, T., Andersson-Engels, S., Einarsdóttír, M. & Svanberg, K. (2007). In vivo optical characterization of human prostate tissue using near-infrared time-resolved spectroscopy, *Journal of Biomedical Optics* 12: 014022.

Swartz, H. (2007). On tissue oxygen and hypoxia, *Antioxidants & Redox Signaling* 9(8): 1111–1114.

Trachtenberg, J., Bogaards, A., Weersink, R., Haider, M., Evans, A., McCluskey, S., Scherz, A., Gertner, M., Yue, C., Appu, S. et al. (2007). Vascular targeted photodynamic therapy with palladium-bacteriopheophorbide photosensitizer for recurrent prostate cancer following definitive radiation therapy: assessment of safety and treatment response, *The Journal of urology* 178(5): 1974–1979.

Van der Veen, N., Van Leengoed, H. & Star, W. (1994). In vivo fluorescence kinetics and photodynamic therapy using 5-aminolaevulinic acid-induced porphyrin: increased damage after multiple irradiations., *British journal of cancer* 70(5): 867.

van Veen, R., Aalders, M., Pasma, K., Siersema, P., Haringsma, J., van de Vrie, W., Gabeler, E., Robinson, D. & Sterenborg, H. (2002). In situ light dosimetry during photodynamic therapy of Barrett's esophagus with 5-aminolevulinic acid, *Lasers in surgery and medicine* 31(5): 299–304.

Vesselov, L., Whittington, W. & Lilge, L. (2005). Design and performance of thin cylindrical diffusers created in Ge-doped multimode optical fibers, *Applied optics* 44(14): 2754–2758.

Ward, J. (2008). Oxygen sensors in context, *Biochimica et Biophysica Acta (BBA)-Bioenergetics* 1777(1): 1–14.

Weersink, R., Bogaards, A., Gertner, M., Davidson, S., Zhang, K., Netchev, G., Trachtenberg, J. & Wilson, B. (2005). Techniques for delivery and monitoring of TOOKAD (WST09)-mediated photodynamic therapy of the prostate: clinical experience and practicalities, *Journal of Photochemistry and Photobiology B: Biology* 79(3): 211–222.

Wilson, B. (2008). Advanced Photodynamic Therapy, *Biophotonics* pp. 315–334.

Wilson, B. & Patterson, M. (1986). The physics of photodynamic therapy, *Physics in Medicine and Biology* 31: 327–360.

Wilson, B., Patterson, M. & Lilge, L. (1997). Implicit and explicit dosimetry in photodynamic therapy: a new paradigm, *Lasers in Medical Science* 12(3): 182–199.

Yu, G., Durduran, T., Zhou, C., Zhu, T., Finlay, J., Busch, T., Malkowicz, S., Hahn, S. & Yodh, A. (2006). Real-time in situ monitoring of human prostate photodynamic therapy with diffuse light, *Photochemistry and photobiology* 82(5): 1279–1284.

Zaak, D., Frimberger, D., Stepp, H.,Wagner, S., Baumgartner, R., Schneede, P., Siebels, M., KN "UCHEL, R., Kriegmair, M. & Hofstetter, A. (2001). Quantification of 5-aminolevulinic acid induced fluorescence improves the specificity of bladder cancer detection, *The Journal of urology* 166(5): 1665–1669.

Zhu, T., Finlay, J. & Hahn, S. (2005). Determination of the distribution of light, optical properties, drug concentration, and tissue oxygenation in-vivo in human prostate during motexafin lutetium-mediated photodynamic therapy, *Journal of Photochemistry and Photobiology B: Biology* 79(3): 231–241.

Zhu, T., Li, J., Finlay, J., Dimofte, A., Stripp, D., Malkowicz, B. & Hahn, S. (2006). In-vivo light dosimetry of interstitial PDT of human prostate, *Proceedings of SPIE*, Vol. 6139, p. 61390L.

Data Acquisition

Edited by Michele Vadursi

ISBN 978-953-307-193-0
Hard cover, 344 pages
Publisher Sciyo
Published online 28, September, 2010
Published in print edition September, 2010

The book is intended to be a collection of contributions providing a birdâ€™s eye view of some relevant multidisciplinary applications of data acquisition. While assuming that the reader is familiar with the basics of sampling theory and analog-to-digital conversion, the attention is focused on applied research and industrial applications of data acquisition. Even in the few cases when theoretical issues are investigated, the goal is making the theory comprehensible to a wide, application- oriented, audience.

How to reference

In order to correctly reference this scholarly work, feel free to copy and paste the following:

Emma Henderson, Benjamin Lai and Lothar Lilge (2010). Spatial-Temporal Dose Metric Sampling for Explicit Photodynamic Therapy, Data Acquisition, Michele Vadursi (Ed.), ISBN: 978-953-307-193-0, InTech, Available from: http://www.intechopen.com/books/data-acquisition/spatial-temporal-dose-metric-sampling-for-explicit-photodynamic-therapy

INTECH
open science | open minds

InTech Europe
University Campus STeP Ri
Slavka Krautzeka 83/A
51000 Rijeka, Croatia
Phone: +385 (51) 770 447
Fax: +385 (51) 686 166
www.intechopen.com

InTech China
Unit 405, Office Block, Hotel Equatorial Shanghai
No.65, Yan An Road (West), Shanghai, 200040, China
中国上海市延安西路65号上海国际贵都大饭店办公楼405单元
Phone: +86-21-62489820
Fax: +86-21-62489821

IntechOpen